Nanoscale Advances

ROYAL SOCIETY OF CHEMISTRY

PAPER

View Article Online
View Journal | View Issue

Cite this: *Nanoscale Adv.*, 2025, **7**, 4591

Development of cost-effective fluorescent carbon nanoparticles as security ink for anticounterfeiting and fingerprint visualization

Shiv Rag Mishra, [ac] Tuhin Mandal, [ac] Ashish Kumar Ghosh[cd] and Vikram Singh *[abc]

Anticounterfeiting and latent fingerprinting have become ever-growing global demands, impacting national economies, defence and various technological fields. This has led to an increasing need for photoluminescent materials that are nontoxic, highly luminous, photostable, more sensitive and low-cost. However, there is a lack of research reports that offer a detailed exploration of photoluminescent materials for both anticounterfeiting and latent fingerprinting. Thus, we explored waste pistachio shell biomass-derived tunable fluorescent carbon nanoparticles as an invisible/security ink for latent fingerprint visualization and anticounterfeiting labels. Three levels of security characteristics for fingerprint analysis were investigated to enable a more comprehensive exploration of the synthesised fluorescent carbon nanoparticles. The invisible distinctive impression of the ridges, grooves, and furrows of the fingers was visible on the thin layer chromatographic plate after fluorescent carbon nanoparticle-based ink was applied to the finger under UV-light excitation. The anticounterfeiting study was performed after labelling the prepared ink on Whatman filter paper, TLC plates, PVA films and Indian currency to investigate its diversified applications. This study provides a new prospect for low-cost and non-toxic photoluminescent carbon nanoparticles as invisible ink for security, encryption, and labels.

Received 17th April 2025
Accepted 2nd June 2025

DOI: 10.1039/d5na00370a

rsc.li/nanoscale-advances

1 Introduction

Invisible inks are stimuli-responsive optical materials composed of luminophores that exhibit specific responses to ultraviolet (UV) or infrared (IR) illumination. These inks are invisible under natural visible light, but they luminesce and become visible under UV & IR irradiation. This encryption technique of invisible ink is utilised for anticounterfeiting, fingerprint visualisation and many more purposes.[1–5] Anticounterfeiting is a potent tool that makes original products arduous to copy and it easy to verify essential and valuable products, including bank currency, pharmaceuticals, agrochemical products, luxurious items, tickets, certificates, and documents.[6,7] These days, counterfeiting of high-security products, valuable items, currency, and certificates is a global problem that challenges companies, governments, and customers. This is why anti-counterfeiting techniques are crucial for authenticating trademarked products and protecting intellectual property rights. Barcodes, holograms, special codes, product information and QR codes with luminescent encryption are valuable techniques that provide additional security and address the counterfeiting problem.[8–10]

Like anticounterfeiting, latent fingerprinting is also a powerful technique for providing distinct and crucial physical evidence at a crime scene, identifying a particular individual and offering investigative clues to help track the criminal. When a hand comes into contact with anything, the wrinkled patterns of the finger will leave a mark on the surfaces of the objects.[11–13] Fingerprints have ridges, grooves and furrows that are unique to each person and do not change throughout life. These fingerprints on the surface of objects are called latent fingerprints and effectively serve as a trace of evidence for identifying a person. The morphology of the fingerprints is categorised into three distinct points: the first level signifies the overall details, such as whorls, arches and loops; the second level represents minutiae points, including bifurcation and termination of ridges, and the third level signifies specific levels such as pores, furrows, ridges, and grooves.[14,15] Among them, the second and third levels of fingerprint features are most valuable and suitable for particular identification. However, identifying their characteristics, especially the third-level features, which express a high level of security and require high-resolution methods, is challenging.[16,17] Typically, latent fingerprints are invisible to the naked eye; for visualization, it is necessary to develop

[a]*Environment Emission and CRM Section, CSIR-Central Institute of Mining and Fuel Research Dhanbad, Jharkhand, 828108, India*

[b]*Analytical Sciences Group, ASSIST Division, CSIR-Indian Institute of Toxicology Research, Vishvigyan Bhawan, 31, M.G. Marg, Lucknow, Uttar Pradesh, 226001, India. E-mail: vikram.singh05@iitr.res.in*

[c]*Academy of Scientific and Innovative Research (AcSIR), Ghaziabad, 201002, India*

[d]*Resource Quality Assessment Division, CSIR-Central Institute of Mining and Fuel Research, Dhanbad, Jharkhand 828108, India*

visualization techniques. Several methods, such as the powder approach, chemical treatment, *etc.*, are adopted to make the latent fingerprints of an individual visible.[18,19] However, their uses are hindered by their weak contrast, toxicity, low selectivity, and expensive and contamination problems. Photoluminescent nanomaterial-based invisible ink has caught the attention of people who want to extract fingerprints with high contrast, colour accuracy, small size, and colour variety. Fluorescent organic dyes, rare earth nanoparticles and semiconductor polymer dots, inorganic metal complexes, *etc.*, have been recently explored as invisible inks, but their use is also limited due to the challenges of their complex synthesis, toxicity, stability issues, and low quantum yield.[20–24]

Fluorescent carbon nanoparticles (CNPs), a type of photoluminescent carbon nanomaterial, arouse growing interest as an invisible ink due to their outstanding functional properties such as low toxicity, good biocompatibility, high stability, excellent quantum yield and cost-effectiveness. These exciting features of fluorescent CNPs make them attractive for multifunctional applications, including photovoltaic, bio-medical, sensor, lighting, display technologies, *etc.*[25–35] The applications of fluorescent CNPs for invisible ink have not been explored much in the literature for broader usage. Additionally, fluorescent CNPs exhibit tunable fluorescent properties that provide extra security features to imitate and duplicate, making them excellent candidates for invisible ink applications. A range of synthetic methods, including hydrothermal, solvothermal, laser ablation, arc discharge and ultrasonication, are employed for the preparation of fluorescent CNPs from distinct chemical precursors such as citric acid, malic acid, trimeric acid, urea, ascorbic acid, fructose, *etc.*[36–38] However, biomass has gained significant attention as a precursor to developing fluorescent CNPs due to its wide availability and pre-existing functional groups.[39–41] The design and synthesis of fluorescent carbon nanoparticles from waste biomass in a green manner is an innovative and cost-effective approach for preparing invisible ink.

Thus, in this study, we choose the pistachio shell as a waste biomass precursor, mainly consisting of carbon, hydrogen, nitrogen, sulphur, and oxygen for synthesising tunable fluorescent CNPs. Herein, tunable fluorescent CNPs were reported from waste pistachio shells using dimethyl sulfoxide as a dispersion medium through mild pyrolysis-assisted ultrasonication. This innovative approach is scalable, combining waste-to-wealth principles, green solvents, and ultrasonication for rapid, eco-friendly fluorescent CNP production compared to previously reported methods. The developed fluorescent CNPs were thoroughly utilized as an invisible ink for latent fingerprint visualization and anticounterfeiting labels under UV-light excitation. A comparative table is mentioned in Table 2, highlighting key parameters between our synthesised fluorescent CNPs and previously reported carbon nanomaterial-based invisible inks. Our developed method stands out by requiring lower temperatures, avoiding toxic chemicals, and reducing synthesis time, offering significant advantages over existing approaches. Furthermore, an anticounterfeiting investigation was conducted after labelling the prepared fluorescent CNP-based ink on Whatman filter paper, TLC plates, PVA films, and Indian currency to study its diversified applications. Three levels of security characteristics for fingerprint analysis were investigated to enable a more comprehensive exploration of the synthesised fluorescent carbon nanoparticles. Additionally, the use of green solvents such as dimethyl sulfoxide, ethanol, and glycerol in the development of fluorescent CNPs and invisible ink provides a safer, biodegradable, and environmentally friendly alternative to traditional organic solvents in UV ink formulations, helping minimize health and ecological risks. Therefore, these findings offer promising possibilities for using fluorescent CNPs as biocompatible and eco-friendlier security ink in the anti-counterfeiting and latent fingerprinting fields, especially in forensic investigations, as both offer improved contrast and greater details in latent prints compared to traditional methods, making them highly effective tools for forensic analysis.

2 Experimental study

2.1 Materials

The pistachio shells (Pistacia vera L.) were collected from used dry fruits. High-quality filter papers and chemicals, such as dimethyl sulphoxide and ethanol, were procured from Sigma-Aldrich Ltd. Double-distilled water was prepared in our laboratory to make water-dispersed materials. Glycerol was purchased from SRL Pvt Ltd, India, for making invisible ink.

2.2 Instrumentation

Shape and morphological characterisation of prepared CNPs was done by using a Thermo Fisher Scientific Talos F200X G2, a high-resolution transmission electron microscope (HRTEM). A Shimadzu Iraffinity-1S infrared spectrophotometer is used to detect the various surface functionalities. The X-ray photoelectron spectroscopic study was also performed using the PHI 5000 VersaProbe III equipment to determine various surface functionalities, and the elemental compositions of CNPs were confirmed by X-ray photoelectron spectroscopy using PHI 5000 VersaProbe III equipment, which has a monochromatic argon

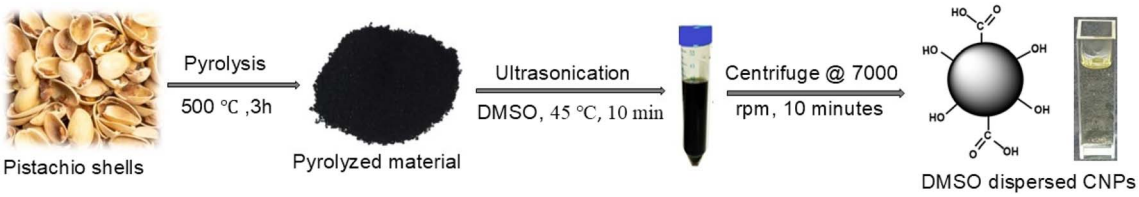

Scheme 1 Schematic representation for the synthesis of blue-emitting CNPs using ultrasonication of the pyrolyzed material from pistachio shells.

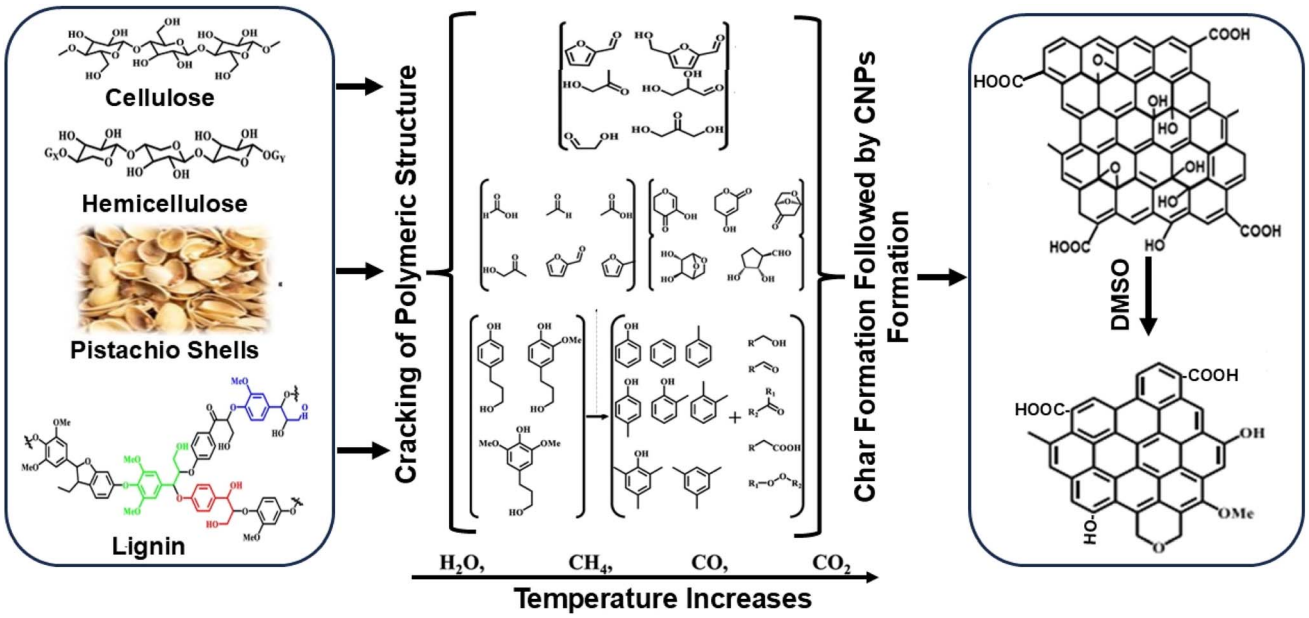

Scheme 2 Possible mechanism of the development of CNPs *via* the ultrasonication of pistachio shell-derived biochar.

gun in the range of 5–5000 eV. The UV-visible and steady-state fluorescence studies have been carried out using Agilent Cary 5000 UV-vis-NIR and Hitachi F-7000 fluorescence spectrophotometers (150 W xenon lamps), respectively.

2.3 Synthesis of fluorescent CNPs

We used waste pistachio shells (Pistacia vera L.) as a carbon-rich precursor and DMSO as a dispersion medium using an ultrasonication method. Pistacia vera peels were pyrolyzed in a volatile matter (VM) furnace for 3.0 h at 500 °C in the absence of oxygen to decompose the biomass into combustible gases and carbon-rich (>80%) bio-char.[42] Then, the pyrolyzed material (biochar) was powdered finely with the help of a mortar and pestle. After that, from the powdered biochar, 0.1 g of powdered material is dispersed in 30 mL of DMSO and then ultrasonicated at 45 °C for 10 minutes. Then, the solution is filtered through Whatman 40 filter paper and centrifuged at 7000 rpm. After that, we get the clear CNP solution with a concentration of 0.2 mg mL^{-1} (Scheme 1). The prepared CNP solution emitted cyan blue fluorescence under 365 nm UV light excitation.

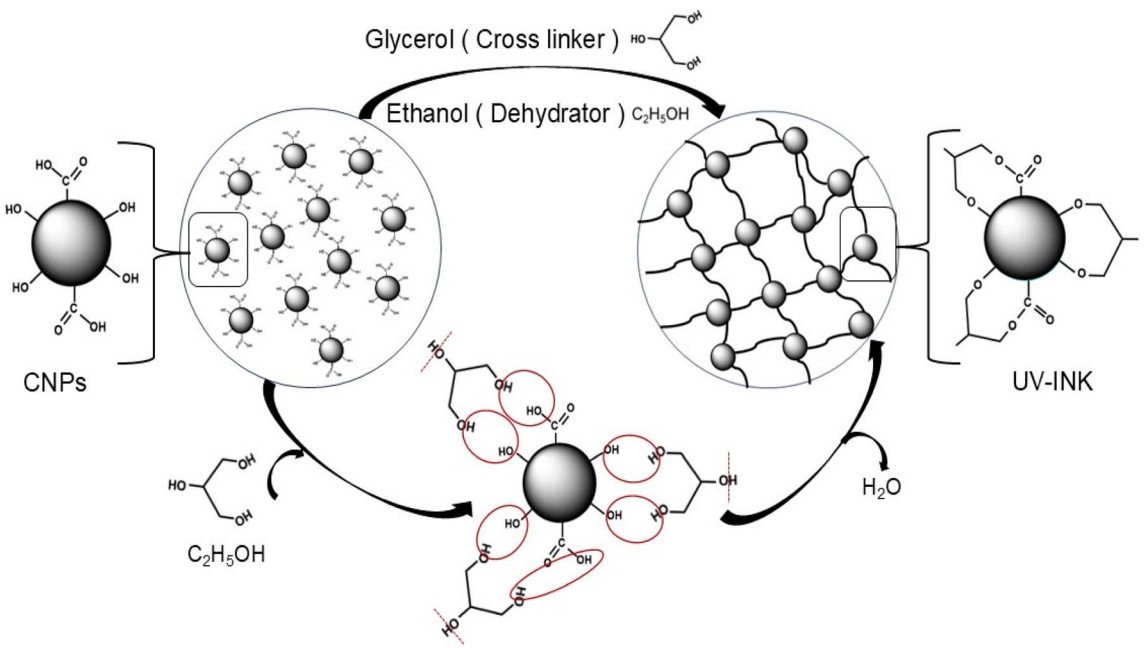

Scheme 3 Mechanism of formation of security UV ink from CNPs and a glycerol and ethanol mixture.

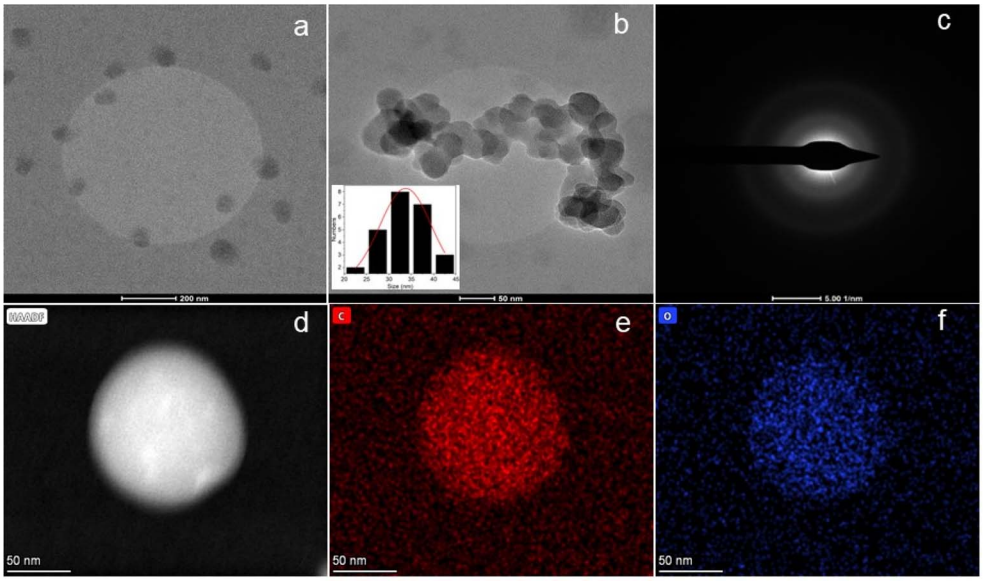

Fig. 1 HRTEM images of CNPs: (a) low magnification; (b) high magnification with a particle size distribution plot in the inset; (c) the SAED pattern showing a dull ring and (d–f) HADF mapping of carbon and oxygen, respectively.

2.4 Mechanism of formation of CNPs

The mechanism of formation of CNPs involves the cracking of the polymeric structure of the shell skeleton, resulting in the generation of some oxygenate forms such as furan, pyran derivatives, and phenolic compounds, together with small amounts of acid, alcohols, and light aromatic hydrocarbons *via* dehydration. These species are repolymerised at higher temperatures to form graphene oxide-like structures, followed by CH_4, CO and CO_2 elimination. When a carbonised material is ultrasonicated with DMSO as a dispersion medium, a reduction reaction occurs and a graphene oxide-like structure is reduced to an amorphous carbon skeleton-like moiety (Scheme 2).

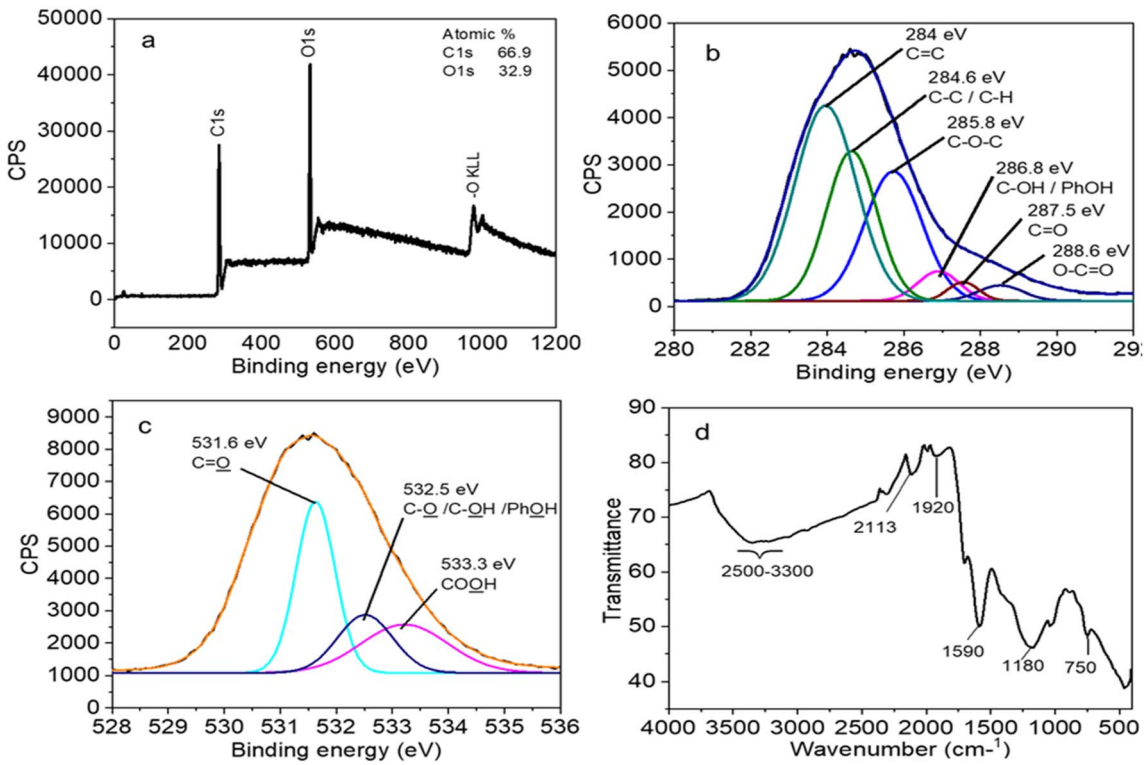

Fig. 2 (a) Full scan of the XPS survey spectra with the atomic percentage of CNPs; (b) high-resolution C 1s full spectrum; (c) high-resolution O 1s full spectrum; (d) FTIR spectra of CNPs.

2.5 Preparation of security ink using fluorescent CNPs

For application as invisible ink, the components of that ink must be invisible under natural light. The invisible ink was fabricated using CNPs, ethanol and glycerol as the dehydrator, evaporator and viscosity modifier binders in a 2 : 1 : 1 ratio, respectively. Ethanol acts as a dehydrator to accelerate the evaporation, helping the paper dry out quickly. The inclusion of glycerol enhances both wet and rub resistance while also maintaining the ink's viscosity and consistency. It serves as an effective viscosity modifier and cross-linking agent.

2.6 Formation mechanism of security ink

Invisible ink was prepared by mixing CNPs with glycerol and ethanol. Glycerol has a trifunctional structure, and it can serve as a non-toxic cross-linking agent through the interaction between its hydroxyl groups and surface functional groups (–OH and –COOH) of the CNPs. As a dehydrating agent, ethanol helps eliminate water molecules during the reaction process. The possible mechanism of the formation of UV ink is presented schematically in Scheme 3.

3 Results and discussion

3.1 Morphological and topographical characterisation

The size distribution and morphology of the prepared CNPs were observed using high-resolution transmission electron microscopy (HRTEM). The HRTEM images in Fig. 1(a) and (b) confirmed the spherical shape with asymmetrical distributions of the CNPs. The size distribution plot in Fig. 1(b) confirmed that the average size of the CNPs ranged from 30 to 36 nm. The faint ring patterns observed in Fig. 1(c) using the selected area electron diffraction (SAED) analysis further confirmed the amorphous nature of the CNPs. The high-angle annular dark-field (HAADF) analysis from the scanning transmission electron microscopy study indicated the elemental composition of CNPs, which is mainly composed of carbon and oxygen (Fig. 1a–f).

3.2 Surface functionalisation study

The XPS spectroscopic measurement was performed to analyze the elemental state and chemical bonds in the as-synthesized CNPs. Fig. 2(a) shows the full range XPS spectra with two different peaks at 284.6 and 532.2 eV, which correspond to the atomic C 1s and O 1s, with an existence ratio of 66.9% and 32.9% for C and O, respectively.[43] The high-resolution scan of the atomic C 1s confirmed the six-bonding state, such as C=C at 284 eV, C–C/C–H at 284.6 eV, C–O–C at 285.8 eV, C–OH/Ph–OH at 286.8, C=O at 287.5 and O–C=O at 288.6 eV (Fig. 2b). The other scan of the atomic O1s confirmed the three different bonding states, such as C=O at 531.6 eV, C–O/C–OH/Ph–OH bonds at 532.5 eV, and COOH at 533.3 eV (Fig. 2c).

The FTIR study further confirmed the presence of various surface functional groups of CNPs. The very broad peak in the 3300–2500 cm^{-1} region, centred near 3000 cm^{-1}, corresponds to the O–H stretch of the carboxylic acid groups. The peak at 1590 cm^{-1} confirms the presence of the C=C stretch of the aromatic ring and at 1180 cm^{-1} corresponds to the –C–O stretch of phenolic groups (Fig. 2d).

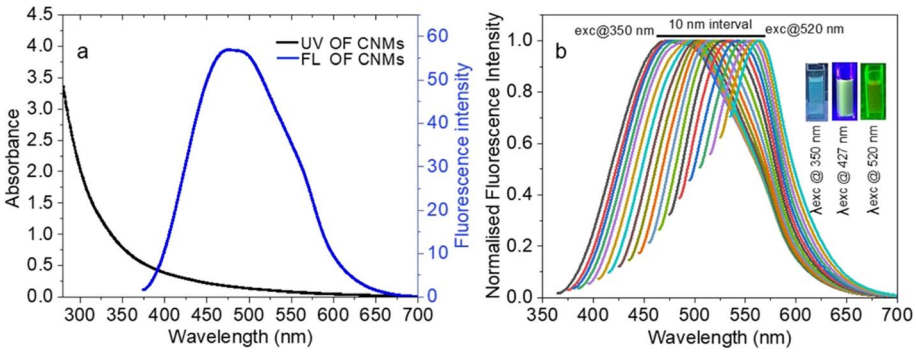

Fig. 3 (a) Absorption and emission spectra of the blue fluorescent CNPs ($\lambda_{exc} = 370$ nm and $\lambda_{em} = 475$ nm); (b) normalized excitation-dependent emission spectra of DMSO dispersed CNPs, [CNPs] = 0.2 mg mL^{-1}, with the inset showing the blue, yellow and green emitting CNPs under the excitation of 350 nm, 427 nm and 520 nm wavelengths, respectively.

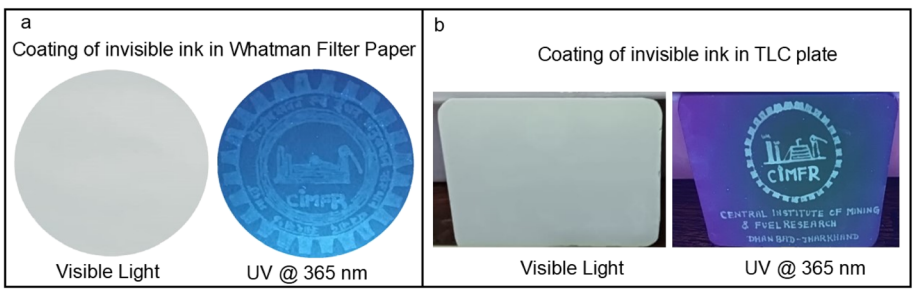

Fig. 4 Photographs of loaded information using the CNP-based invisible ink on (a) the Whatman filter paper and (b) on the TLC plate under natural light and 365 nm UV-light irradiation.

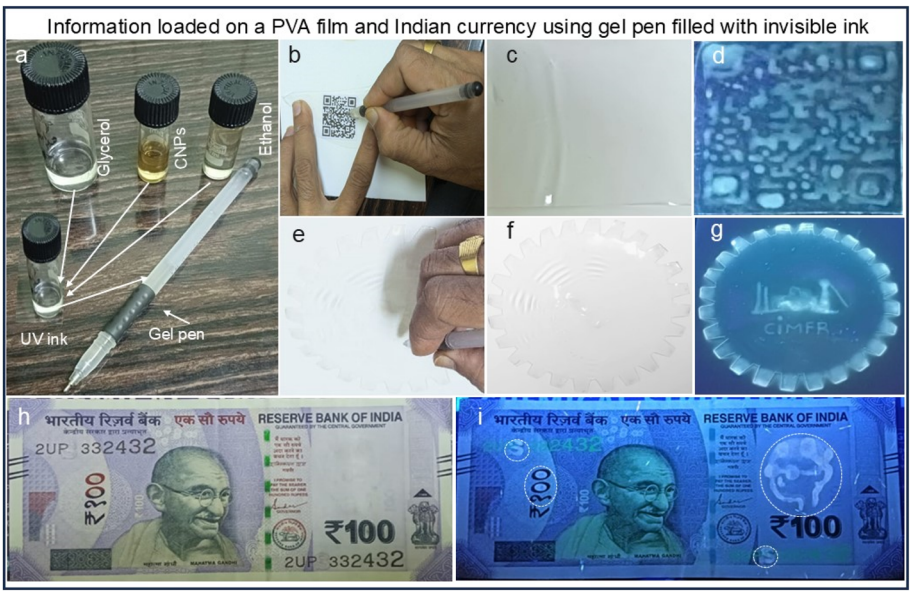

Fig. 5 (a) Components of UV ink (b) loaded information (bar coding) on a PVA film, (c) encrypted information on the PVA film under daylight, (d) decrypted information on the PVA film under 365 nm UV-light irradiation, (e) loaded information (CIMFR logo) on the PVA film, (f) encrypted information under daylight, (g) decrypted information under 365 nm UV-light irradiation, (h) encrypted information on Indian currency under daylight and (i) decrypted information on Indian currency under 365 nm UV-light.

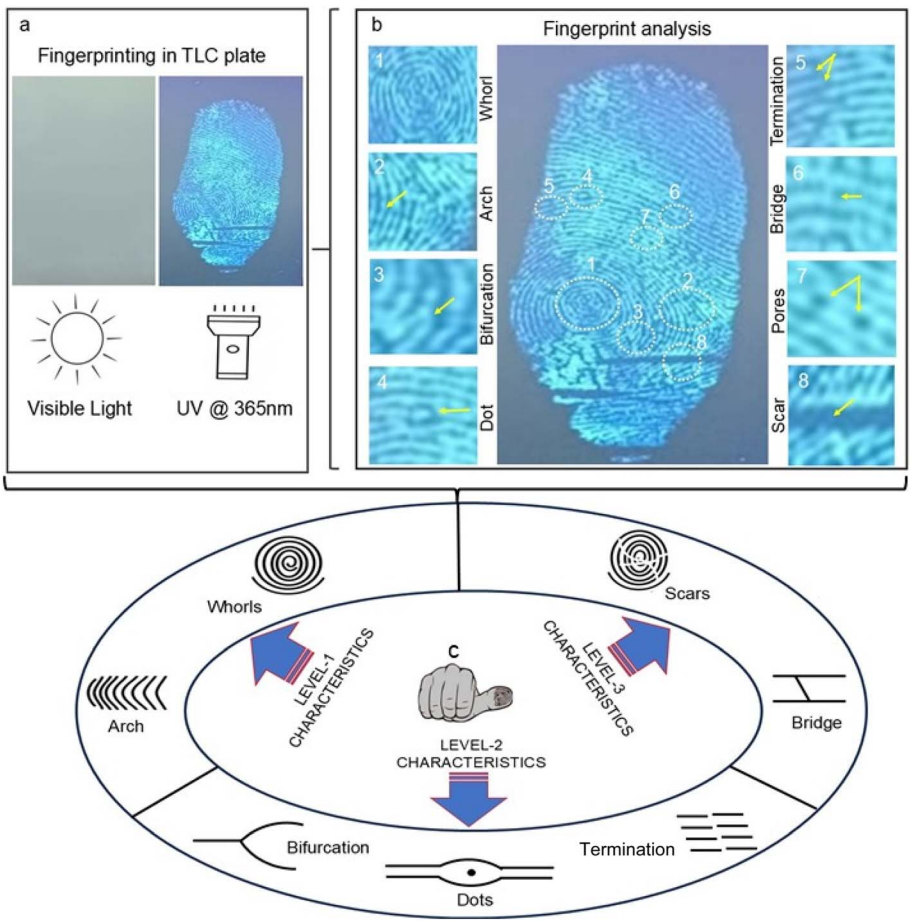

Fig. 6 (a) Image of the fluorescent CNP based invisible ink-loaded fingerprint on the TLC plate under visible light and UV excitation, respectively. (b) The expended finger impressions on the TLC plate showing individual characteristics showing level-I details (whorls and arches), level-II details (bifurcations, dots, terminations, *etc.*) and level-III details (sweat pores and scars) with high-level security under UV light illumination. (c) Classification of the three levels of characteristics of fingerprint analysis.

3.3 Photophysical study

The photophysical characterisation of the synthesised CNPs was conducted in a polar aprotic DMSO solution at 25 °C. A clear, dispersed CNP solution with a 0.2 mg mL^{-1} concentration showed characteristic absorption in the 280–600 nm range with a peak at 280 nm. The absorption band at 280 nm indicates the distinctive peak of phenolic π systems or the π–π^* transition of oxygen functionalities, which involves trapping excited-state energy by the surface states. The shoulder peak at 325 nm is due to the n–π^* transition of the carbonyl and carboxyl functionalities of the CNPs. The CNP solution showed intense blue fluorescence, with an emission peak at 475 nm (Fig. 3a). To investigate the tunable behaviour of DMSO-dispersed CNPs, the CNP solution was scanned at the excitation starting from 350 to 520 nm wavelengths with 10 nm intervals, and emission response was recorded from 370 to 700 nm. A remarkable bathochromic shift was observed in the normalised emission spectra of the CNP solution (Fig. 3b). A real-time colour change of the CNP solution under different excitations was also seen in the inset of Fig. 3b.

4 Applications as invisible ink

4.1 Anticounterfeiting analysis

The anticounterfeiting analysis was carried out after preparing the CNP-based invisible ink solution, described in Section 2.5. Furthermore, to test the ink's compatibility and versatile applications, various writing and templating tools, including Whatman filter paper, thin layer chromatography (TLC) plates, a polyvinyl alcohol (PVA) film, and Indian currency, were used for information loading.

The encrypted information, as "Central Institute of Mining and Fuel Research (CIMFR) and its logo", was written on the Whatman filter paper (Fig. 4a) and TLC plate (Fig. 4b) using a commonly used gel pen. The writing was invisible under natural light, while it became visible under 365 nm UV illumination (Fig. 4a and b).

In addition, when this invisible ink was applied to encrypt the barcode (Fig. 5b–d) and CIMFR logo (Fig. 5e–g) information on the PVA film, the information was visible, which emitted bright blue fluorescence under UV illumination. The invisible ink was also employed in Indian currency to write hidden information using an invisible ink-filled gel pen. The information was also invisible under natural light and visible under UV light illumination (Fig. 5h–5i).

4.2 Fingerprint analysis

Fingerprint analysis is the most effective tool for representing an individual's identity in investigative practices, such as crime scene investigations, twin studies, inheritance research, and forgery cases as evidence. Fingerprint analysis involves three levels of characteristics, including levels 1, 2 and 3, as shown in

Table 1 Usefulness of prepared fluorescent CNPs for fingerprint visualisation based on the level of characteristics and their limitations

Levels of characteristic	Description/key feature	Limitations
Level-1 (arches and whorls)	(1) Useful for initial screening of fingerprints to determine the global pattern type and orientation	(1) Not sufficient to differentiate individuals because they represent only the general pattern. Thus, level-2 & 3 characteristics are essential for accurate fingerprint analysis and matching
	(2) These can be used to quickly specify the search for a fingerprint within a large database	(2) It cannot establish a reliable correspondence between live and spoof fingerprint samples
	(3) Imparts image orientation and enhancement, making it easier to analyse other levels of details	
Level-2 (bifurcations, dots and terminations)	(1) These are also known as minutiae. By concentrating on minutiae, we can achieve higher accuracy in fingerprint matching	(1) These can be difficult to extract if ridges are smudged and damaged (wear and tear on the skin)
	(2) Useful for quick identification of individuals based on minutiae points, where dots or bifurcations are used to compare fingerprint patterns	(2) The reliable identification of level 2 features can be challenging when only a portion of the fingerprint is available
	(3) Various automated fingerprint identification systems trust level-2 minutiae to match fingerprints	(3) If the fingerprint image is in low resolution, it may not be easy to discern the subtle details of level 2 characteristics
Level-3 (scars, bridges, and pores)	(1) It shows microscopic features such as pores, bridges and scars, which provide unique details in fingerprint analysis	(1) Level 3 characteristics are magnificent and require high-resolution fingerprint imaging (*e.g.*, 1000 dpi) for proper extraction
	(2) These have a crucial role in fingerprint analysis by imparting abundant and large details of fingerprint structures, enhancing accuracy, and providing the identification of individuals	(2) Extracting and matching level-3 characteristics have some challenges. Pores can be complex and computationally intensive
	(3) Provides additional information for problematic fingerprint recognition and even donor profiling (age, sex, race, *etc.*)	(3) High-resolution requirements pose a challenge, particularly when handling latent fingerprints left at crime scenes, which may be of poor quality due to smudging or partial prints

Table 2 A comparative table highlighting key parameters between our synthesized fluorescent CNPs and previously reported carbon nanomaterial-based invisible inks

S. No.	Fluorescent carbon nanomaterials	Precursor	Solvents	Temp (°C)	Time (min)	References
1	Carbon dots	Wasted coffee grounds	Diluted nitric acid	220	1200	Hong *et al.*[44]
2	Carbon dots	Turtle shell	Water	500	300	Guo *et al.*[45]
3	Carbon dots	Glutathione	Water	220	1080	Zhang *et al.*[46]
4	Carbon quantum dots	Mopan persimmon pulp	Water	150	240	Ma *et al.*[47]
5	Carbon dots	Dried spinach leaf powder	Water	180	480	Wang *et al.*[48]
6	Carbon dots	Citric acid	Ethylene-diamine and water	220	300	Kalytchuk *et al.*[49]
7	Carbon nanoparticles	*Meta*-phenylenediamine	Ethanol	180	1440	Luo *et al.*[50]
8	Carbon dots	*Meta*-phenylenediamine and phosphoric acid	Ethanol	180	240	Wang *et al.*[51]
9	Carbon dots	Crystal violet	Sulfuric acid and water	200	120	Yang *et al.*[52]
10	Carbon nanoparticles	Pistachio (pistacia) shell	Dimethyl sulfoxide	45	10	This study

Fig. 6. The detailed description of these characteristics is given in Table 1.

For fingerprint analysis, the fluorescent CNP-based invisible ink was first applied to the finger, and then the fingerprint was initially developed on the TLC plate. The encrypted fingerprint on the TLC plate was invisible under natural light but became visible under 365 nm UV light (Fig. 6a). Later, we demonstrated the first, second and third levels of fingerprint security details such as whorls, arches, bifurcations, terminations, dots, bridges, scars, and pores to determine the selectivity and contrast of the fluorescent CNPs. Using the emission of the fluorescent CNP-based inks, we displayed the second- and third-level finger pattern details such as whorls, arches, bridges, islands, deltas, lakes, scars, terminations, bifurcations, dots, hooks, and pores as shown in Fig. 6b. Classification of the three levels of characteristics of fingerprint analysis is shown in Fig. 6c.

As shown in the expanded images, both the papillary ridges and the furrows were revealed clearly with sharp edges, resulting in high selectivity due to the small size and optimal adsorptive properties of fluorescent CNP-based inks. Although we haven't explored them yet, the tunability properties of the developed fluorescent CNPs are crucial factors in developing different excitation decryption methods, which will be valuable for future studies.

5 Conclusions

In summary, this study demonstrates a novel approach to synthesise biocompatible fluorescent CNPs from biomass waste, Pistacia vera peel, as a carbon-rich source. Later, the prepared fluorescent CNPs are utilized as an invisible ink for anti-counterfeiting and fingerprint applications. The anticounterfeiting investigation was conducted by applying the prepared fluorescent CNP-based ink onto Whatman filter paper, TLC plates, PVA films, and Indian currency to explore its diverse applications. The anticounterfeiting investigation was conducted by labelling the prepared fluorescent CNP-based ink on various writing and templating tools to explore its diversified applications, and it was observed that the ink successfully encrypted coded information under natural visible light and decrypted it under UV light. In the latent fingerprint investigation, the fluorescence-based invisible ink showed highly contrasted, distinctive impressions of the fingers' ridges, grooves and furrows. This analysis supports future advancements in forensic science, particularly in the identification and analysis of evidence. Additionally, these UV-sensitive inks can be seamlessly integrated into high-security documents, such as passports, currency, and certificates, to provide an advanced, tamper-evident layer of protection against counterfeiting. These findings present promising opportunities for CNP-based invisible ink for anti-counterfeiting and latent fingerprinting in secret communications and forensic analysis. In our future work, we aim to address the limitations of these findings and explore their broader applications through new and innovative approaches (Table 2).

Data availability

The data that support the findings of this study are available from the corresponding author, upon reasonable request.

Conflicts of interest

The authors declare no conflict of interest.

Acknowledgements

VS thanks CSIR-Central Institute of Mining and Fuel Research, Dhanbad, for funding (MLP-190/2024-25) and providing the facilities. SRM thanks Dayanand Vedic College, Orai (Jalaun), for providing the financial support and necessary help. The authors acknowledge the central research facility, the Indian Institute of Technology (ISM) Dhanbad, for the HRTEM, XPS, and UV-visible analyses. The CSIR-IITR communication number is IITR/SECC-PME/MSS/2025/022.

References

1 J. Lee, S. G. Kong, T.-Y. Kang, B. Kim and O.-Y. Jeon, *Forensic Sci. Int.*, 2014, **236**, 77–83.
2 P. Kumar, S. Singh and B. K. Gupta, *Nanoscale*, 2016, **8**, 14297–14340.
3 K. Muthamma, S. Acharya, D. Sunil, P. Shetty, A. A. Abdul Salam, S. D. Kulkarni and P. J. Anand, *J. Colloid Interface Sci.*, 2024, **653**, 209–219.
4 V. Singh, B. Gorbel, S. Chatterjee, P. Sen and V. Verma, *Mater. Lett.*, 2022, **309**, 131446.
5 A. Abdollahi, A. Dashti, M. Rahmanidoust and N. Hanaei, *Sens. Actuators, B*, 2022, **372**, 132649.
6 L. Sun, L. Li and L.-J. Fan, *ACS Appl. Nano Mater.*, 2024, **7**, 26164–26174.
7 A. Abdollahi, H. Roghani-Mamaqani, B. Razavi and M. Salami-Kalajahi, *ACS Nano*, 2020, **14**, 14417–14492.
8 K. Muthamma, D. Sunil and P. Shetty, *Appl. Mater. Today*, 2021, **23**, 101050.
9 W.-K. Tsai, Y.-S. Lai, P.-J. Tseng, C.-H. Liao and Y.-H. Chan, *ACS Appl. Mater. Interfaces*, 2017, **9**, 30918–30924.
10 X. Yu, H. Zhang and J. Yu, *Aggregate*, 2021, **2**, 20–34.
11 C. Yuan, M. Li, M. Wang, H. Cao and T. Lin, *Electrochim. Acta*, 2021, **390**, 138798.
12 M. Wang, M. Li, A. Yu, J. Wu and C. Mao, *ACS Appl. Mater. Interfaces*, 2015, **7**, 28110–28115.
13 R. Bahadur, M. K. Kumawat, M. Thakur and R. Srivastava, *J. Lumin.*, 2019, **208**, 428–436.
14 A. A. Ansari, K. M. Aldajani, A. N. AlHazaa and H. A. Albrithen, *Coord. Chem. Rev.*, 2022, **462**, 214523.
15 R. Dhaneshwar, M. Kaur and M. Kaur, *Egypt. J. Forensic Sci.*, 2021, **11**, 33.
16 D. K. Williams, R. L. Schwartz and E. G. Bartick, *Appl. Spectrosc.*, 2004, **58**, 313–316.
17 L. Xu, Y. Li, S. Wu, X. Liu and B. Su, *Angew. Chem., Int. Ed.*, 2012, **51**, 8068–8072.
18 G. S. Sodhi and J. Kaur, *Forensic Sci. Int.*, 2001, **120**, 172–176.
19 M. Li, J. Xu, Q. Zheng, C. Guo and Y. Chen, *Anal. Chem.*, 2022, **94**, 7238–7245.
20 R. M. Snari, R. A. Pashameah, N. M. Alatawi, A. T. Mogharbel, Z. A. Al-Ahmed, H. M. Abumelha and N. M. El-Metwaly, *Microsc. Res. Tech.*, 2022, **85**, 3871–3881.
21 T. P. Nguyen, H. P. Dang, L. G. Nguyen and C. D. Le, *Opt. Mater.*, 2024, **157**, 116296.
22 M. Zuo, W. Qian, T. Li, X.-Y. Hu, J. Jiang and L. Wang, *ACS Appl. Mater. Interfaces*, 2018, **10**, 39214–39221.
23 X. Long, J. Wang, Y. Ma and S. Wu, *Colloids Surf., A*, 2023, **676**, 132136.
24 Z. Song, T. Lin, L. Lin, S. Lin, F. Fu, X. Wang and L. Guo, *Angew. Chem., Int. Ed.*, 2016, **55**, 2773–2777.
25 K. Singh, T. Mandal, U. P. Pandey and V. Singh, *ACS Biomater. Sci. Eng.*, 2025, **11**, 742–773.
26 S. R. Mishra, T. Mandal, R. N. Senapati and V. Singh, *Carbon Lett.*, 2025, **35**, 1067–1079.
27 T. Mandal, S. Rag Mishra, A. Banerjee, G. Firoz, R. Poddar and V. Singh, *ChemistrySelect*, 2024, **9**, e202402666.
28 S. R. Mishra, T. Mandal, S. Sahu, M. Mishra, R. N. Senapati and V. Singh, *ACS Omega*, 2024, **9**, 38916–38924.
29 T. Mandal, S. R. Mishra, M. Kumar and V. Singh, *Sustainable Energy Fuels*, 2024, **8**, 5638–5671.
30 T. Mandal, S. R. Mishra, K. Singh, H. Agarwalla, R. E. Masto, M. Kumar and V. Singh, *J. Nanopart. Res.*, 2023, **25**, 125.
31 K. S. Rawat, V. Singh, C. P. Sharma, A. Vyas, P. Pandey, J. Singh, N. M. Gupta, M. Sachdev and A. Goel, *J. Imaging*, 2023, **9**, 19.
32 V. Singh, K. S. Rawat, S. Mishra, T. Baghel, S. Fatima, A. A. John, N. Kalleti, D. Singh, A. Nazir, S. K. Rath and A. Goel, *J. Mater. Chem. B*, 2018, **6**, 3366–3371.
33 D. Bharathi, R. H. Krishna, V. Singh, N. Kottam and B. Siddlingeshwar, *J. Lumin.*, 2017, **190**, 328–334.
34 V. Singh and A. K. Mishra, *Sens. Actuators, B*, 2016, **227**, 467–474.
35 S. K. Tiwari, M. Bystrzejewski, A. De Adhikari, A. Huczko and N. Wang, *Prog. Energy Combust. Sci.*, 2022, **92**, 101023.
36 T. Mandal, S. R. Mishra and V. Singh, *Nanoscale Adv.*, 2023, **5**, 5717–5765.
37 D. Bharathi, B. Siddlingeshwar, R. H. Krishna, V. Singh, N. Kottam, D. D. Divakar and A. A. Alkheraif, *J. Fluoresc.*, 2018, **28**, 573–579.
38 P. Lamichhanae, M. M. Devadiga, S. Das, N. Wang and S. K. Tiwari, *Next Mater.*, 2025, **6**, 100285.
39 T. Mandal, A. K. Ghosh, S. R. Mishra, S. K. Pandey and V. Singh, *Nanoscale Adv.*, 2023, **5**, 4269–4285.
40 V. Singh, S. Chatterjee, M. Palecha, P. Sen, B. Ateeq and V. Verma, *Carbon Lett.*, 2021, **31**, 117–123.
41 S. R. Mishra, T. Mandal, P. Kumar, V. Verma, R. N. Senapati, M. Kumar and V. Singh, *Surf. Interfaces*, 2025, **69**, 106770.
42 S. C. Peterson and B. J. Chisholm, *J. Compos. Sci.*, 2024, **8**, 482.
43 J. C. G. da Silva, J. L. F. Alves, W. V. A. Galdino, R. Moreira, H. J. José, R. F. de Sena and S. L. F. Andersen, *Environ. Sci. Pollut. Res. Int.*, 2018, **25**, 21420–21429.
44 W. T. Hong and H. K. Yang, *Optik*, 2021, **241**, 166449.
45 J. Guo, H. Li, L. Ling, G. Li, R. Cheng, X. Lu, A.-Q. Xie, Q. Li, C.-F. Wang and S. Chen, *ACS Sustain. Chem. Eng.*, 2020, **8**, 1566–1572.
46 H. Zhang, L. Sun, X. Guo, J. Xu, X. Zhao and Y. Xia, *Appl. Surf. Sci.*, 2023, **613**, 155945.
47 H. Ma, L. Guan, M. Chen, Y. Zhang, Y. Wu, Z. Liu, D. Wang, F. Wang and X. Li, *Chem. Eng. J.*, 2023, **453**, 139906.
48 S. Wang, H. Zhao, J. Yang, Y. Dong, S. Guo, Q. Cheng, Y. Li and S. Liu, *ACS Omega*, 2023, **8**, 6550–6558.
49 S. Kalytchuk, Y. Wang, K. Poláková and R. Zbořil, *ACS Appl. Mater. Interfaces*, 2018, **10**, 29902–29908.
50 S. Luo, H. Deng, J. Chen, S. Xu, Y. Tian, F. Huang, H. Wang, J. Cui and J. Chen, *Chem. Eng. J.*, 2025, **510**, 161778.
51 Y. Wang and S. Wu, *Mater. Sci. Eng., B*, 2025, **319**, 118355.
52 L. Yang, S. Liu, T. Quan, Y. Tao, M. Tian, L. Wang, J. Wang, D. Wang and D. Gao, *J. Colloid Interface Sci.*, 2022, **612**, 650–663.